Archaeomagnetic versus luminescence methods: the case of an Early Byzantine ceramic workshop in Thessaloniki, Greece

Elina Aidona, George Polymeris, Pierre Camps, Despina Kondopoulou, Nikos Ioannidis, Konstantinos Raptis

HAL Id: hal-01823896

https://hal.umontpellier.fr/hal-01823896v1

Submitted on 25 Oct 2024

Archaeomagnetic versus luminescence methods: the case of an Early Byzantine ceramic workshop in Thessaloniki, Greece.

Elina Aidona[1], George S. Polymeris[2], Pierre Camps[3], Despina Kondopoulou[1], Nikos Ioannidis[1], and Konstantinos Raptis[4]

[1]Department of Geophysics, School of Geology, Aristotle University of Thessaloniki, P.O. Box 352-1, 54124 Thessaloniki, Greece
[2]Institute of Nuclear Sciences, University of Ankara, Beşevler, 06100 Ankara, Turkey
[3]Geosciences Montpellier, CNRS and University Montpellier, 34095 Montpellier, France
[4]Ephorate of Antiquities of Thessaloniki, P.O. Box 18432, 54003 Thessaloniki, Greece

Abstract

In this contribution, we present a combined archaeomagnetic and luminescence study of archaeologically dated structures. The investigated area is a ceramic workshop comprising several Early Byzantine kilns. Based on (a) the archaeological–anthropogenic stratigraphy of the site, (b) the structural characteristics of the kilns and (c) the few ceramic findings revealed within their context, the operation of this brick and tile factory is approximately dated between the middle of the fifth century until the first decades of the sixth century AD. Three of the well-preserved workshop kilns have been studied archaeomagnetically. The full vector of the geomagnetic field, accompanied by rock magnetic analyses of the studied material, has been defined. The archaeomagnetic study revealed similar directions among the three kilns indicating and confirming their contemporary use. Additionally, several luminescence measurements were obtained on material from the same kilns. The dating of the site was performed with both methods. The archaeomagnetic dating is convergent with the archaeological estimation only when its upper limit is considered. Concerning the luminescence dating, the calculated ages (corrected for anomalous fading and for the 40K content) with their standard deviations are convergent with the archaeological estimations for the first kiln, while for the other two, the results seem to be incompatible. The possible factors that provoked this divergence are thoroughly discussed.

Keywords

Introduction

Archaeomagnetism—a discipline of geomagnetism—deals with the study of the geomagnetic field variation through historical and prehistorical times. The method is based on two fundamental principles: (a) the archaeological clay features contain magnetic minerals that can record the geomagnetic field under certain conditions: the material has to be exposed to high temperatures (at least 500–600 °C) and, during the cooling process, it can acquire a remanent magnetization being parallel and proportional to the Earth's ambient magnetic field, and (b) the direction and the strength of the Earth's magnetic field are changing in both time and place. Taking into consideration the above principles, it is possible to build, for a certain area, secular variation curves (SVCs) for the three elements of the geomagnetic field, i.e. declination, inclination and intensity, using well-dated, by independent methods, artefacts such as 14C or luminescence [thermoluminescence (TL) and/or optically stimulated luminescence (OSL)]. The comparison of the obtained direction and intensity of the studied archaeological material with these reference curves can be used for the relative dating of the structure.

Archaeomagnetism has gained an importance during the last decades especially in Europe. Several studies have been performed in order to estimate the variation of the geomagnetic field and its significance in terms of dating fired archaeological structures, as described in the previous paragraph. Several geomagnetic models have been proposed for either regional (Pavón-Carrasco et al. 2010, 2014) or global (Donadini et al. 2009; Korte et al. 2009) datasets, enabling the dating of broad archaeological periods starting from the Neolithic period. During the last years, the archaeomagnetic method is considered as a valuable dating tool, not only in cases where other more traditional dating methods failed to estimate the age of the structures but also due to its capacity to date directly the structures themselves and not findings they contain.

The same development in obtaining new archaeomagnetic data is observed in Greece during the last decade. Several studies have been performed covering the data acquisition from archaeological burnt artefacts from the Neolithic (Aidona and

Kondopoulou 2012; Fanjat et al. 2013) up to the Byzantine (Evans 2006; De Marco 2007; Kondopoulou et al. 2015) period. Recently, De Marco et al. (2014) presented a compilation of all available directional Greek data, resulting in the construction of the updated Greek SVC for the last 4500 years. From the distribution of the Greek archaeomagnetic dataset, significant gaps are observed for historical and prehistorical times. More specifically, around 1200–450 BC, there are no available archaeomagnetic directional data, while for the historical times, from 400 AD and onwards, the coverage is very poor.

Towards further enriching the already available SVC and improving these datasets for poorly resolved periods, accumulating new high-quality data remains an important key objective. Nevertheless, the archaeomagnetic method requires an independent age evaluation in order to establish the SVC but also for comparison and cross-check reasons. Different authors highlight the importance of independent dating techniques resulting in the better reliability of the archaeomagnetic data, since age uncertainties can provide an additional error to the construction of SVCs and regional or global models (Pavón-Carrasco et al. 2014). For quite an extended period, among the plethora of the established archaeometric dating techniques, 14C has been repeatedly used (Maniatis 2014 and references therein). The other physical method, luminescence, in both terms of thermoluminescence (TL hereafter) as well as optically stimulated luminescence (OSL hereafter), besides a reliable dating tool, presents also an important advantage for supporting archaeomagnetic studies.

Luminescence dating works on the principle that materials containing naturally occurring radioactive isotopes, such as uranium, thorium, rubidium and potassium, or which lie in close proximity to other materials containing these radioactive elements, are subject to low levels of radiation (Walker 2005). Radiation ionizes the atoms of the materials, thus creating free electrons and positive ions (holes), which diffuse through the material until they finally get trapped in specific defects (hereafter termed as traps) of the crystal lattice. Among these traps, some can be stable enough to store the electrons for extremely long time intervals, depending upon specific physical characteristics of the material. The electrons trapped in these stable (deep) traps could be released, producing luminescence (Furetta 2003) if they are externally stimulated to,

inside the laboratory. Stimulation usually occurs either by heating or by the action of light. In the former case, one deals with TL, while in the latter, with OSL.

The total number of trapped charges and, consequently, the intensity of the luminescence light are proportional to the total radiation energy absorbed by the materials and, therefore, to the time subjected to irradiation (Aitken 1985, 1998). However, every time that the material is subjected to either prolonged heating (as in the case of firing) or intense light exposure (as in the case of sunlight), accidentally or intentionally, electrons are evicted and traps are emptied. In that case, the material is considered to be totally zeroed (Liritzis et al. 2013a). Afterwards, it can start accumulating energy in the form of trapped electrons in order to refill the empty traps again. Thus, the amount of trapped charge forms a clock that starts ticking from the moment the mineral is buried and protected by light or from heating. The age of the sediment is given by the ratio of the equivalent dose (De, in Gy units), standing as the amount of irradiation dose from β or γ radiation, which is needed in order to obtain a luminescence signal identical to that resulting from natural radiation exposure (Huntley and Lian 1999) over the annual dose rate (DR, in Gy/year units).

In a nutshell, archaeomagnetic and luminescence techniques date exactly the same event, the last heating of clay artefacts baked at high temperature, such as kilns and pottery. For this reason, both aforementioned techniques have been already used as complementary, since their combination can offer a powerful tool for cross-checked dating of archaeological baked clay artefacts (Tema et al. 2013, 2015; Kondopoulou et al. 2015).

In the framework of the present contribution, our team focuses on the study of a large ceramic—brick and tile producing—workshop, which operated during the Early Byzantine period 1.5 km to the west of the western walls of Thessaloniki, at the crossing of Yannitson and Mazaraki streets (Raptis 2012a, b). Medieval Thessaloniki, being diachronically the second and only constantly active—apart from Constantinople—urban centre of the Byzantine Empire and the main commercial hub of the Illyricum, controlled both the official and unofficial productive and mercantile activities throughout the European lands of the Byzantine territory and played an important sociopolitical and economical role during the Middle Ages (Raptis 2015b). Apart from the ceramic workshop studied here and two others already sampled by our team

(Aidona et al. 2010; Aidona et al., in preparation), more than six ceramic workshops have been unearthed and studied in the western part of Thessaloniki during the last 30 years (Raptis 2011a, b, 2015a; Hasaki and Raptis 2016). Numerous ceramic and pottery production areas are also reported from Byzantine excavations in Athens, Delphi and Corinth (Raptis 2011a; Hasaki and Raptis 2016). It is therefore surprising that so few archaeomagnetic data exist after 400 AD, and these derive mostly from directions. Intensity data are almost missing between 500 AD and 1000 AD and are quite dispersed afterwards. A recent study on Greek ceramics dated from the middle fourth century to the early seventh century AD revealed increasing intensity values ranging from 51 to 60 μT (Genevey et al. 2017). This period of time is thus a well-justified target, and all opportunities to study it must be seized.

Site description

The studied ceramic workshop (Fig. 1a) was unearthed during a rescue excavation at the margins of the western cemetery of the Late Antiquity of Thessaloniki. The workshop was producing ceramic building materials and was organized in an argillaceous context, overlying a flood layer which covered several graves dated between the second century and the mid fourth century AD. The stratigraphy suggests that during the workshop installation, the burials were not visible and the layers were only slightly disturbed by the opening of subterrestrial firing chambers. Therefore, the workshop postdates the end of the fourth century AD.

The workshop establishment consisted of clay deposits, a clay levigation tank and five kilns arranged in groups of two. The kilns (Fig. 1b), all circular or elliptic, present different types of brick-built supports of their escharas—that is the perforated firing floor—and therefore belong to all known subtypes of type 1 as classified by Raptis (2011a). Their dimensionsrangefrom4.50m×3.90mto2.25m×2mforthe three elliptic kilns and a diameter of 2.40 m for the circular one. All the kilns are structurally similar, with the internal part of the firing chamber coated with a thick clay layer whereas brick and tile fragments cemented with clay or mud were used for the praefurnium and the eschara. In all cases, the upper part of the kilns was not preserved (Raptis 2015a).

Based on the morphological and structural characteristics of the kilns and the stratigraphy of the site, the operational period of the workshop could be chronologically attributed to the Late Antiquity, most probably from the middle of the fifth until the first decades or the middle of the sixth century AD.

Only three out of the five kilns were sampled since the biggest one, kiln II (Fig. 1b), was preserved for restauration and kiln V was seriously damaged. The sampled parts of the three kilns will be separately described in the following paragraph.

Sampling, methods and instrumentation

The three kilns (I, III and IV; hereafter referred as YA1, YA3 and YA4) have been sampled for the archaeomagnetic and the luminescence study. The samples were taken oriented using both magnetic and sun compasses.

Kiln YA1 (Fig. 1b), slightly pear-shaped displayed a floor coated by vitrified ashes and small ceramic sherds. Eight samples have been retrieved.

Kiln YA3 (Fig. 1b), semi-elliptic, features an axial pilar for supporting the eschara, preserved up to 90 cm. Traces of vitrification were visible on its perimeter and covered also the floor. Ten samples were taken from this kiln.

Finally, kiln YA4 (Fig. 1b), circular, displayed a central pilar for supporting the eschara and, apart from the vitrification on its external surface, a vitrified soil covered the floor, reaching about half of the height of kiln's walls. Ten samples have been also retrieved from this kiln. The extended vitrification strongly favors high temperatures achieved in all three kilns. In all cases, the main concern was to select representative samples that were uniformly distributed over the structures.

The collected samples have been first treated in the laboratory with a non-magnetic rock hardener (Wacker Stone Strengthener OH) for consolidation, and following this, the archaeomagnetic specimens have been prepared in a form of cylinders with a height of 2.2 cm and a diameter of 2.5 cm.

The measurements of the magnetization were performed with a Molspin Minispin spinner magnetometer (Molspin, Newcastle, UK). The magnetic cleaning of the samples

was performed with both a Molspin MSA2 AF tumbler demagnetizer (Molspin, Newcastle, UK) for AF demagnetization and a MMD80 oven for thermal treatment. Isothermal remanent magnetization (IRM) was imparted by means of an impulse magnetizer (ASC IM10-30) at a maximum field of 1.2 T. In order to better determine the magnetic carriers, a composite three-axis IRM was imparted along three orthogonal axes consecutively at 2, 0.5 and 0.2 T (z-, y- and x-axis, respectively) in selected samples and they were subjected to thermal demagnetization up to temperatures of 520 °C (Lowrie 1990).

The anisotropy of low-field magnetic susceptibility was measured on an MFK1 Kappabridge (Gams Palaeomagnetic Laboratory, Leoben University, Austria). High-temperature monitoring of magnetic susceptibility (thermomagnetic analysis) was performed with an MFK1 Kappabridge (Gams Palaeomagnetic Laboratory, Leoben University, Austria) and a KLY3 Kappabridge coupled with a CS3 furnace (Palaeomagnetic Laboratory, IPGP, Paris, France). The experiment was carried out in air by heating the samples up to 600 °C (heating curve) and subsequent cooling to room temperature (cooling curve).

The absolute palaeointensity of selected samples has been determined with the multispecimen with domain state corrections (MSP-DSC) protocol, which corresponds to the multispecimen technique (Biggin and Poidras 2006; Dekkers and Böhnel 2006) including both normalization by the overprinted partial thermoremanence magnetization (pTRM) fraction (f) of the natural remanent magnetization (NRM) and correction for multidomain bias (Fabian and Leonhardt 2010). The multispecimen protocol is based on the physical assumptions that a linear relation exists between the laboratory field and the pTRM imparted in the sample and that no pTRM is acquired if the heating/cooling cycle is performed in a zero field. In this latter case, provided that no alteration took place during the laboratory heating, the magnetizations (m1, m2 and m3) acquired in the MSP-DSC protocol are equal, leading to a fitting line anchored to the point (0,−1) in the regression analysis (Fabian and Leonhardt 2010). The experiment was performed with a homemade furnace (FUReMAG, patent no. 1256194) developed by the palaeomagnetic group at the University of Montpellier. This infrared furnace heats standard-sized palaeomagnetic samples quickly and uniformly. During heating and cooling, the magnetic field is applied along the NRM direction with a precision of less

than 1° (Tema et al. 2016). According to the MSP-DSC protocol, the heating temperature should be high enough in order to contain a sufficient fraction of the TRM (at least 20%) and, at the same time, low enough to prevent chemical alteration. According to the thermal demagnetization results of the present study, we chose a dwell temperature of 350 °C to impart the laboratory pTRM. A total number of 13 brick samples (three samples from kiln YA1, five from kiln YA3 and five more from kiln YA4) were subjected to TL dating, according to the multigrain, multiple aliquot, TL-based, additive dose procedure in TL (MAAD TL; Aitken 1985, 1998; Liritzis et al. 1997, 2013a; Wagner 1998; Lian and Huntley 2001). Nevertheless, for cross-checking reasons, three brick samples from kilns YA3 and YA4 were also dated with the single-aliquot regenerative dose protocol by OSL (SAR OSL; Murray and Wintle 2000; Liritzis et al. 2013a).

All TL measurements were carried out at the Nuclear Physics Laboratory of the Physics Department, Aristotle University of Thessaloniki, Greece, by means of a Littlemore-type 711 setup, with a P/M tube (EMI 9635QA bialkali; Sb K–Cs), a thermocouple-type 90/10 Ni/Cr and 97/03 Ni/Al and a heat filter transmitting in the 320–440-nm range. In all cases, a beta test dose was provided by a $90Sr/90Y$ beta source delivering 1.72 Gy/min. All TL measurements were performed in nitrogen atmosphere up to a maximum temperature of 500 °C at constant heating rate of 2 °C/s in order to avoid significant temperature lag. OSL measurements were performed using a Risø TL/ OSL-DA-20 reader, equipped with a $90Sr/90Y$ beta source delivering 4.5 Gy/min. The reader is fitted with a 9635QA photomultiplier tube. The detection optics consisted of a 7.5-mm Hoya U-340 ($\lambda p \sim 340$ nm, FWHM 80 nm) filter, transmitting in the 280–380-nm region, with maximum transmittance (57%) at 330 nm. Blue light-emitting diodes (LEDs, 470 ± 30 nm) were used for stimulation, emitting 40 mW/cm2 at the position of the sample. All OSL measurements were performed at the continuous wave configuration (CW-OSL), for 100 s at 125 °C with the LED power held at 90% power at 125 °C. For infrared laser stimulation (IRSL), the stimulation wavelength is 875 (±40) nm and the maximum power is $\sim$135 mW/cm2 (Bøtter-Jensen et al. 1999a, b).

The annual dose rate was calculated based on the decay of naturally occurring radionuclides inside the clay matrix, i.e. 40K, 232Th and natural U, along with cosmic rays, which provide a constant source of low-level ionizing radiation, within the historical time frame considered (Prescott and Hutton 1994). Uranium-235 (and, consequently, U-

238) and thorium-232 were measured by alpha counting employing the pairs technique assuming U equilibrium (Liritzis and Vafiadou 2012). These measurements were performed using a 7286 Low-Level Alpha Counter, Littlemore Sci. Eng, Co. (Oxford), a PM tube-type EMI 6097B and a ZnS detector. 40K was estimated by using scanning electron microscopy coupled with electron-dispersive X-ray spectroscopy (SEM-EDX) for the kilns with laboratory codes YA3 and YA4, while for kiln YA1, using micro-X-ray fluorescence (μ-XRF). Dose rate calculations were made using the conversion factors of Liritzis et al. (2013b).

Results

Rock magnetism

Rock magnetic experiments are a prerequisite for any archaeomagnetic investigation since they provide important information about the magnetic carriers, and therefore, they give valuable evidence for the suitability of the studied material to accurately record a thermoremanent magnetization.

The anisotropy of the magnetic susceptibility was measured on 25 selected specimens from all samples, indicating that the studied material is weakly anisotropic. The degree of anisotropy (P') shows a mean value of 4%, which can be considered as insignificant. This outcome is not surprising as our samples consist of baked clays that proved to display very low anisotropy values (less than 5%) (Kovacheva et al. 2009).

Nine samples from the three kilns have been subjected to stepwise IRM acquisition procedure. As shown in Fig. 2a, the majority of the samples seem to reach the saturation level below 1.2 T, indicating the presence of low coercivity magnetic minerals. However, there are few cases where saturation is not reached at 1.2 T, indicating the coexistence of a high coercivity magnetization component.

This is further supported by the thermal demagnetization of the composite IRM imparted to ten specimens from the three kilns. Representative diagrams of the magnetization decay during the demagnetization (Fig. 2b) display the dominance of a soft fraction of magnetization which is eliminated before 600 °C (kilns YA1 and YA3) or before 500 °C (YA4), while the intermediate and hard components are negligible.

Thermomagnetic analysis has been performed on 20 specimens. Representative examples are shown in Fig. 2c. In general, samples from kiln YA1 show a very reversible magnetic susceptibility versus temperature behavior. The majority of the thermomagnetic curves thus indicate the absence of chemical alterations during heating. All samples seem to lose their magnetization at temperatures ranging from 520 to 580 °C, confirming the occurrence of magnetite-like magnetic minerals. Samples from the other two kilns (YA3 and YA4) show a similar behavior with a good reversibility. The presence of high coercivity minerals cannot be ruled out for YA4 while such minerals are more prominent for YA3.

Additionally, the Lowrie–Fuller test (Lowrie and Fuller 1971) has been applied to eight samples from kiln YA1 for which the performed mineralogical analysis, already described, clearly displays dominance of magnetite-type carriers. Among the eight cases, four are compatible with possible MD grains carrying the magnetization, two SD grains and two possible PSD ones (Fig. 2d).

Archaeomagnetic analysis

Directional results

The NRM directions before laboratory treatment are well grouped, i.e. the Fisherian concentration parameter (k) being 33, 95 and 95 for kilns YA1, YA3 and YA4, respectively. This grouping indicates that the majority of the samples have accurately recorded the ancient geomagnetic field. Few outliers have been observed, and these samples were not considered for further analysis.

The magnetic cleaning of the samples revealed the presence of one stable component of magnetization in all cases (Fig. 3). In total, 76 specimens from the three kilns were demagnetized with both methods: alternative field (AF) and thermal (TH) treatment in zero field. During the AF demagnetization, samples from YA1 and YA4 could fully eliminate their magnetization up to 100 mT, while for few samples from YA3, the demagnetization was not completed up to 100 mT (Fig. 3a).

During the thermal cleaning, all samples were totally demagnetized beyond to 580 °C and no different behaviors regarding the three kilns were observed (Fig. 3b).

The direction of the characteristic remanent magnetization (ChRM) was calculated separately for each kiln and is presented in Table 1 and Fig. 4. As the archaeological evidence supports the synchronous function of the three kilns and as the obtained archaeomagnetic results are similar, we calculate a mean value of the site presented in Table 1.

Archaeointensity results

The archaeointensity was determined by means of the multispecimen protocol as proposed by Fabian and Leonhardt (2010). Seventeen samples from the three kilns were used. At first standard selection, criteria were applied in order to separate the more reliable data from those of poor quality. These criteria are essentially based on three considerations.

1. The fraction of the NRM replaced by the laboratory pTRM during multiple heatings must be between 20 and 80% of the total NRM. In this interval, the fraction is large enough to be accurately measured and well below a total TRM.
2. The maximum angle between the NRM left after the pTRM acquisition and the total NRM is fixed at 10°.
3. The relative alteration error (εalt) (see equation 19 in Fabian and Leonhardt 2010) must be lower than 10%.

Obviously, in the present case, this selection appears inefficient to screen out individual data of poor quality as attested by the dispersion in Fig. 5a.
The regression analysis is performed by means of weighted least squares, with a model anchored to the theoretical point (0,−1). Doing this, it is normal to find the largest residuals from the model for data determined with the largest error bars. More surprisingly, we observed that data with the largest residuals correspond to those samples for which the NRM fractions are the lowest (Fig. 5a). Without any objective reason except this simple observation, we decided to discard these data by keeping only the ones determined with a NRM fraction between 0.65 and 0.8. Doing this, the regression analysis is by far of higher quality (Fig. 5b). This differentiation leads to the conclusion that our samples show mineralogical heterogeneities resulting in different

unblocking temperatures, the large error bars reflecting significant chemical changes during the laboratory heatings (difference between m1 and m4 intensities).

Archaeomagnetic dating

For the archaeomagnetic dating, the Matlab tool by Pavón- Carrasco et al. (2011) was used. The dating was performed on the basis of the regional model SCHA.DIF.3K which predicts the geomagnetic field at the place of interest, avoiding in this way possible relocation errors. At a first step, every kiln was dated separately using the obtained directional results. For YA1, the archaeomagnetic dating yields an age interval from 191 to 413 AD. The second kiln YA3 yields ages ranging from 113 to 441 AD, while the last one, YA4, has a similar age interval from 105 to 432 AD. The archaeomagnetic dating is constant in all three kilns, indicating that the studied material recorded reliably the last use of the kilns as the obtained archaeomagnetic directions used for the dating from each kiln separately lead to the same results. Since the archaeointensity was determined for the three kilns as a whole (according to the archaeological information and the identical archaeomagnetic directional results), we chose to date the three kilns with the full vector of the magnetic field as it is derived from their mean value of the direction and the intensity (Table 1). The final archaeomagnetic dating is displayed in Fig. 6. As shown, the mean age value resulting from the calculated geomagnetic field does not differ from the individual dating of the kilns; the estimated age interval is from 167 to 411 AD. This outcome has to be compared to the available archaeological information which puts a terminus post quem at ca. 350–400 AD, with most findings indicating a later dating, during the second half of the fifth century.

Luminescence analysis and results

Regardless of the luminescence protocol applied for all samples, typical treatment and preparation were undertaken, in subdued red filtered light conditions, including the following steps (Kondopoulou et al. 2015; Liritzis et al. 2015; Tema et al. 2015):

a. Removal of the 0.5-cm-thick outer layer from each sample in the laboratory in order to eliminate the light-subjected portions.

b. Application of the typical chemical procedure described by Vieillevigne et al. (2007) for sample preparation.

c. Extraction of grains within the grain size range 4–12 μm, suspension in acetone and final precipitation onto 1-cm- diameter aluminium discs (Zimmerman 1971).

Results of MAAD TL procedure

In the framework of MAAD TL, for each of the studied samples, 16 separate discs/aliquots were prepared and subsequently divided into four different groups, consisting of four aliquots each. Mass reproducibility for all samples was kept within ±3%. Samples were irradiated into groups of four discs at each dose. Three different artificial doses of 5, 10 and 15 Gy were attributed, plus a zero Gy additive dose, corresponding to the natural TL (NTL hereafter) signal. Figure 7 presents the typical MAAD TL analysis results for the sample YA4-2; these results are representative for all the samples that were the subject of the present study. The plot in Fig. 7a presents typical additive dose glow curves, each one being the mean value of at least three independently measured glow curves.
The TL signal presents a linear response over increasing doses. Therefore, only linear fittings were performed to the dose–response curves. This linearity should be strongly established; this is the reason why, in Fig. 7b, the dose–response slope (S) is plotted versus temperature for the three different additive doses applied. This slope is calculated ac
cording to the following formula (Polymeris et al. 2012):

$$S = [(NTL+\beta_i) - (NTL)] / \beta_i \qquad (1)$$

where (NTL + β_i) denotes the corresponding glow curves after the corresponding additive dose has been administered, so the preceding subtraction takes place for each data point. One S curve corresponding to each additive dose is yielded. In the case of linearity, these three curves should coincide, as the case presented in Fig. 7b throughout the entire temperature region of the glow curve. The inset of this plot

presents a representative example of additive (squares) and regenerated TL (diamonds) buildup curves for the temperature of 320 °C; in the latter case, the dose–response during the corresponding second glow TL dose–response curve after applying low doses (diamonds) indicates the absence of supra-linearity in the low-dose region (Zimmerman 1971; Aitken 1985). Supralinearity correction, I, is equal to zero since the second glow TL dose–response passes from the origin of both axes.

Equivalent doses were estimated over a wide temperature region, in units of Gy, according to the following equation:

$$D_e = NTL / S \ (Gy) \qquad (2)$$

A typical plot of De against glow curve temperature is presented in Fig. 7c. Wide equivalent dose plateaus were yielded, with the equivalent doses being obtained as the mean values of the best plateaus for each sample. Errors derived mainly from the uncertainties in curve fitting, are ±1σ and were calculated by standard error propagation analysis. A summary of the TL data is given in Table 2.

Results of SAR OSL procedure

The single-aliquot regenerative dose protocol, introduced by Murray and Wintle (2000), was used in order to estimate the equivalent dose using OSL. In the SAR OSL technique, the signal intensity of an aliquot of extracted grains (called natural OSL) is recorded and then the same aliquot is subjected to a series of subsequent laboratory irradiations with a calibrated radiation source and OSL measurements. Each disc was exposed to infrared radiation for 100 s at 50 °C before the OSL, in order to reduce the malign influence of feldspar grain to the signal (Wallinga 2002; hereafter referred as post IR OSL). The procedure is similar to the double SAR procedure of Banerjee et al. (2001), containing additional SAR steps in order to minimize the need for chemical separation. The summary of the post IR OSL data is also given in Table 2.

TL fading corrections

The OSL signal after the IRSL cleaning, termed as post IR OSL, is dominated by the quartz signal (Banerjee et al. 2001; Roberts and Wintle 2001; Zhang and Zhou 2007), as

Table 2 is further revealing these De values are somehow overestimated compared to the corresponding De values measured using TL. This slight discrepancy is attributed to the presence of anomalous fading in the case of TL measurements. Since quartz was not chemically isolated, the anomalous fading in TL was also estimated. A close look at the additive glow curves of Fig. 7a indicates that the so-called 110 °C peak of quartz is obvious. Nevertheless, the other well-established TL glow peaks of quartz are not prominent, indicating that the rest of the glow curve consists of one broad continuum, typical for a feldspathic dominated signal. In order to calculate the fading-corrected equivalent doses, the method suggested by Huntley and Lamothe (2001) was used, including the calculation of the fractional decrease of the luminescence intensity over a decade, g, according to (Aitken 1985). According to the results yielded, each kiln indicates an individual g value, being 1.37 (±0.10)% per decade for the case of YA3 and 1.85 (±0.12)% per decade for the case of YA4. Surprisingly, the TL of kiln YA1 yielded negligible fading; therefore, no fading correction was applied to kiln YA1. These latter values were used in order to correct the MAAD TL De values. The corrected values, as presented in Table 2, are in better agreement with the corresponding OSL De values.

Dose rate estimation

Due to the fact that the grain size fraction of 4–12 μm was used, the annual dose can be considered as the sum of contributions to the dose from alpha, beta and gamma radiations. Similarly, as described in Tema et al. (2015), the following assumptions were adopted: (a) the contribution of the gamma rays mainly arises from the main body of the kiln and (b) uranium, thorium and potassium concentrations are uniformly distributed all over the kilns. The radioactive geochemistries of the samples, along with an outline of the annual dose rate assessment, are presented in Table 2. The water content of the samples was experimentally measured at 15 ± 2%.

As Table 2 further reveals, the potassium (40K) content is really high for kilns YA3 and YA4; the inverse is observed for the uranium component. This high potassium content could be an experimental artefact. In order to check this, two TLD-100 dosemeters were implanted in the sampling site for 45 days, in order to check the gamma dose rate on site. It is worth mentioning that the dose rate assessed by using the TLD-100 dosemeters

was yielded 2 years later than the sampling time for the TL measurements. Moreover, it consists of a unique value for all samples; unfortunately, it was not possible to obtain an individual annual dose rate assessment for each kiln using TLD-100 dosemeters. The resulting dose rate, as this was estimated by using the TLD-100 dosemeters, is not in agreement with the corresponding one assessed by using the uranium, 232Th and 40K contents for kilns YA3 and YA4, while it is much closer to the dose rate estimated for kiln YA1. In other words, the 40K content was overestimated, at least for kilns YA3 and YA4. This experimental drawback was also discussed by Liritzis et al. (2011); these authors have suggested a correction for this severe overestimation of the 40K content, according to their Figure 1. Based on this methodology, the 40K content of every sample was corrected, resulting in a gamma annual dose rate much more compatible with the corresponding one yielded by the TLD-100 dosemeters. Corrected values of both annual dose rate and obtained ages are presented in Table 2.

Furthermore, it is noteworthy that for kilns YA3 and YA4, the error in the 40K content estimation is really high, of the order of 20% or even higher. A typical SEM backscattered image is presented in Fig. 8. For the potassium content estimation using SEM-EDX spectroscopy, each SEM backscattered image was divided into four segments; an independent potassium estimation for each segment was provided, while for each sample, the average of these four measurements stands as the final value for the 40K content, with the corresponding standard deviation indicating the 1σ error value. This latter feature is revealed only for the case of kilns YA3 and YA4; for kiln YA1, the potassium content is quite decreased with very low uncertainty values, indicating a homogeneity in the clay matrix of this kiln.

Luminescence ages

The ages yielded for kiln YA3 are uniform, indicating the following values of 846 ± 125 years before present without the 40K correction as well as 1416 ± 180 years before present after incorporating both the fading and the 40K correction.

Similarly, for kiln YA4, the corresponding ages are 776 ± 145 years before present without the 40K correction as well as 1186 ± 190 years after incorporating both the fading and the 40K correction. The quite large error values at the final ages are

noteworthy and are directly attributed to the quite enhanced error values on the 40K content. On the contrary, for kiln YA1, the age yielded is 1536 ± 100 years before present. In a nutshell, our results expressed as ages AD are presented as mean values in Table 2. For each one of these aforementioned reported age values, the corresponding error does not indicate 1σ over the mean value; errors were yielded according to standard error propagation theory, based on the error of each individual estimation.

Discussion

Evaluation of archaeomagnetic results

The site mean geomagnetic vector obtained from the present study is compared with already existing results from Greece, dated in the same period as well as with regional (SCHA.DIF.3K) and global (ARH3K.1) models. The archeological dating for the settlement is considered to be the corresponding age for the new data (see below) due to its narrower age interval which nevertheless falls within the thermoluminescence range for YA1. As it is shown in Fig. 9, the three elements of the geomagnetic field are in a very good accordance with other published results. More specifically, declination values are identical with the results of Kondopoulou et al. (2015) while inclination values seem to follow the increasing trend and fill the gap among the results of Kondopoulou et al. (2015). When compared with the models, both directional results are slightly shifted but still are within the error bars. The intensity value is in excellent agreement with the global model (ARH3K.1) and with the results obtained from Kondopoulou et al. (2015). A small deviation is observed with the regional model (SCHA.DIF.3K) and the newly presented results from Genevey et al. (2017) which nevertheless remains within the corresponding error bars.

Comparison of the dating techniques

In Fig. 10, both archaeomagnetic and luminescence datings are compared with the archaeological one. The mean age estimation calculated with the archaeomagnetic

data in the present study (164–411 AD) is not in total agreement with the archaeological one, since only the upper limit of the dating can be considered close to the true dating of the site (Fig. 10). The main reason for this discrepancy could be the fact that during this period, a big plateau in declination as well as in the intensity variation curve used for the dating is observed. Even if for the first half of the first millennium AD the archaeomagnetic records are continuous, it seems that the observed variation of the magnetic field is smooth. Thus, the dating of the three elements of the geomagnetic field is mainly controlled by the variation of the inclination. The same feature is also prominent in the Greek SVC, leading to the same dating results. In order to better define the archaeomagnetic dating, we attempted to use the Bulgarian SVC and RenDate software by Lanos (2007), relocating our results to Sofia coordinates. The new age estimation is limited from 400 to 454 AD, still below the archaeological age (around 500 AD) but to a lesser extent than the one calculated with the regional model.

Age estimations obtained by means of the luminescence technique after all necessary corrections are also shown in Fig. 10. It is obvious that the data are not consistent, indicating a different age for each kiln. Only in the case of YA1 a very good agreement with the archaeological age is obtained. In the case of YA3, the convergence is poor and limited to the lower part of the luminescence estimation, while for YA4, a total discordance is observed. Certainly, this latter disagreement could, at first sight, be attributed to the different experimental techniques applied for the 40K estimation. Unfortunately, the application of μ-XRF for the case of the remaining two kilns was not possible, even though it would have been the optimum solution. The main reason for this discrepancy is seen in the large heterogeneity and inhomogeneity of the material in the two kilns (YA3 and YA4). These two features could be easily demonstrated via a rudimentary statistical analysis performed on the SEM-EDX elemental content results of each sample. The mean values and the corresponding standard deviations were yielded for all major elements; these results are presented in Table 3. Even though Si is uniformly distributed, the remaining elements such as Na, 40K and Mg yield a large inhomogeneity. The latter is expressed in terms of the error percentage of the standard deviation, in respect to the corresponding mean value. Especially for kiln YA4, heterogeneity of almost 30% is monitored, indicating also inhomogeneity to the feldspar content.

The mechanism for this effect is known as beta dose heterogeneity or microdosimetric variation (Cunningham et al. 2012). It is caused by the non-uniform distribution of beta emitting radionuclides in the medium, combined with the short range of beta particles, resulting in a beta dose rate that can vary across spatial scales of the order of tens of microns to several millimeters for sediments (Nathan et al. 2003). Beta heterogeneity, in this paper, primarily refers to non-uniformity in the spatial distribution of potassium, since this is the major source of the beta dose rate; nevertheless, a composition or even density variation of the clay matrix could possibly result to spatially dependent variations in a number of parameters affecting the dose rate, such as electron flux density and energy spectra. The only way to assess the influence of microdosimetric variation to dating could be based on a general model of dose rate heterogeneity, through a series of Monte Carlo simulations of energy deposition, in combination with experimental validation (Cunningham et al. 2012). The main outcome of such a simulation would have been the mean dose rate (Cunningham et al. 2011). Even though assessment of the 40K content by the use of SEM EDX is still debatable, the use of this specific technique enabled easy monitoring of beta dose heterogeneity and microdosimetric variation. It should be emphasized that, to the best of the author's knowledge, microdosimetric variation has been reported mostly to dating studies of sediments using single (Ballarini et al. 2006; Mayya et al. 2006) as well as multiple (Liritzis et al. 2010) grain measurements. It is the first time in the literature that this feature is both reported and dealt with for the case of claybased materials.

Conclusions

An extensive archaeomagnetic and luminescence study has been performed on the material provided by sampling three big ceramic kilns belonging to a spacious workshop situated close to the western walls of the Byzantine City of Thessaloniki. The archaeological evidence supports an Early Byzantine Age for its operation, between the second half of the fifth and the first decade of the sixth century AD. The material proved to be very suitable for an archaeomagnetic study, which resulted in the calculation of a

full vector of magnetization (declination, inclination, intensity) since the three kilns are proved to be in use coevally.

The attempt to date the workshop through this vector was partially successful, mostly due to the rather smooth variation of the declination and intensity of the geomagnetic field within the Roman/Early Byzantine periods. A parallel study through both TL and OSL presented also difficulties since only one out of the three kilns could be dated to the period assigned by the archaeological evidence. Convergent independent age assessment has been achieved by luminescence, besides typical drawbacks such as dose rate overestimation due to potassium overestimation by SEM-EDX, anomalous fading and beta dose heterogeneity which, in turn, result to microdosimetric variation. This latter experimental drawback and its detailed examination is novel in the literature for the case of clay-based materials. The present study suggests that a special caution should be given in the future, as new sampling strategies should be introduced in related studies. These would include raw samples of soil collected on site, as well as microdosimetry scanning, applying 40K measurements in the microscale.

As a final step, we used the well-defined age combined from the archaeological estimation (450–530 AD) in order to plot our vector in the geomagnetic field models. The convergence of our new result with the existing ones for the same area and period validates its reliability and further documents this period poorly covered by archaeomagnetic results.

Acknowledgements :

References :

Aidona E, Kondopoulou D (2012) First archaeomagnetic results and dating of neolithic structures in Northern Greece. Stud Geophys Geod 56:827–844.

Aidona E, Kondopoulou D, Alexandrou M, Ioannidis N (2010) Archaeomagnetic studies in kilns from Northern Greece. Bull Geol Soc Greece XLIII(4):1888–1897

Aitken MJ (1985) Thermoluminescence dating. Academic, London Aitken MJ (1998) An introduction to optical dating. Oxford University Press, Oxford

Ballarini M, Wintle AG, Wallinga J (2006) Spatial variation of dose rate from beta sources as measured using single grains. Ancient TL 24:1–8 Banerjee D, Murray AS, Bøtter-Jensen L, Lang A (2001) Equivalent dose estimation using a single-aliquot of polymineral fine grains. Radiat Meas 33:73–94

Biggin AJ, Poidras T (2006) First-order symmetry of weak-field partial thermoremanence in multi-domain ferromagnetic grains. 1. Experimental evidence and physical implications. Earth Planet Sci Lett 245(1–2):438–453. doi:10.1016/j.epsl.2006.02.035

Bøtter-Jensen L, Duller GAT, Murray AS, Banerjee D (1999a) Blue light emitting diodes for optical stimulation of quartz in retrospective dosimetry and dating. Radiat Prot Dosim 84:335–340

Bøtter-Jensen L, Mejdahl V, Murray AS (1999b) New light on OSL. Quat Sci Rev 18(2):303–309

Cunningham AC, Bakker M, van Heteren S, van der Valk B, van der Spek AJF, Schaart DR, Wallinga J (2011) Extracting storm-surge data from coastal dunes for improved assessment of flood risk. Geology 39:1063–1066

Cunningham AC, De Vries DJ, Schaart DR (2012) Experimental and computational simulation of beta-dose heterogeneity in sediment. Radiat Meas 47(11–12):1060–1067

De Marco E (2007) Complete magnetic and archaeomagnetic measurements in archaeological sites: contribution to the SVC for Greece. PhD Thesis Aristotle University of Thessaloniki 293pp

De Marco E, Tema E, Lanos P, Kondopoulou D (2014) An updated catalogue of Greek archaeomagnetic data for the last 4500 years and a directional secular variation curve. Stud Geophys Geodet 58:127–147

Dekkers MJ, Böhnel HN (2006) Reliable absolute palaeointensities independent of magnetic domain state. Earth Planet Sci Lett 248(1–2): 508–517. doi:10.1016/j.epsl.2006.05.040

Donadini F, Korte M, Constable CG (2009) Geomagnetic field for 0–3 ka: new data sets for global modelling. Geochem Geophys Geosyst 10(Q06007):1–28

Evans ME (2006) Archaeomagnetic investigations in Greece and their bearing on geomagnetic secular variation. Phys Earth Planet Inter 159:90–95

Fabian K, Leonhardt R (2010) Multiple-specimen absolute paleointensity determination: an optimal protocol including pTRM normalization, domain-state correction, and alteration test. Earth Planet Sci Lett 207:84–94

Fanjat G, Aidona E, Kondopoulou D, Camps P, Rathossi C, Poidras T (2013) Archaeointensities in Greece during the Neolithic period: new insights into material selection and secular variation curve. Phys Earth Plan Inter 215:29–42

Furetta C (2003) Handbook of thermoluminescence. World Scientific Publishing Co., Singapore

Genevey A, Kondopoulou D, Petridis P, Aidona E, Muller, Blonde F, Gros JS (2017) New constraints on geomagnetic field intensity variations in the Balkans during the Early Byzantine period from ceramics unearthed at Thasos and Delphi, Greece. Journal of Archaeological Science: Reports, in press

Hasaki E, Raptis KT (2016) Roman and Byzantine ceramic kilns in Greece (1st-15th c. CE): continuities and changes in typology and spatial organization of production. Atti del Convegno Internazionale: Archeologia delle produzioni ceramiche nel mondo antico. Spaci, prodotti, strumenti e techniche Genova 1-2.12.2014; 209–229

Huntley DJ, Lamothe M (2001) Ubiquity of anomalous fading in K feldspars and the measurement and correct. Canadian Journal of Earth Science 38(7):1093–1106. doi:10.1139/cjes-38-7-1093

Huntley DJ, Lian OB (1999) Determining when a sediment was last exposed to sunlight by optical dating. In: Lemmen DS, Vance RE (Eds.) Holocene climate and environmental change in the Pallister Triangle: a geoscientific context for evaluating the impacts of climate change on the Southern Canada Prairies. Geological Survey of Canada Bulletin 543: 211–222. Her Majesty the Queen in Right of Canada Catalogue No. M42-534E

Kondopoulou D, Aidona E, Ioannidis N, Polymeris GS, Tsolakis S (2015) Archaeomagnetic study and thermoluminescence dating of Protobyzantine kilns (Megali Kypsa, North Greece). J Archaeol Sci Rep 2:156–168

Korte M, Donadini F, Constable CG (2009) Geomagnetic field for 0–3 ka: 2. A new series of time-varying global models. Geochem Geophys Geosyst 10(Q06008):1–24

Kovacheva M, Chauvin A, Jordanova N, Lanos P, Karloukovski V (2009) Remanence anisotropy effect on the palaeointensity results obtained from various archaeological materials, excluding pottery. Earth Plan Space 61(6):711–732

Lanos P (2007) Bayesian archaeomagnetic dating: the Rendate software. International Union of Geophysics and Geodesy, Perugia

Lian OB, Huntley DJ (2001) Luminescence dating. In: Tracking environmental change using lake sediments. Basin analysis, coring and chronological techniques. vol 1. Kluwer Academic, Dordrecht

Liritzis I, Vafiadou A (2012) Calibration aspects of thick source alpha counter ZnS system. Measurement 45:1966–1980

Liritzis I, Guilbert P, Foti F, Schvoerer M (1997) The temple of Apollo (Delphi) strengthens new thermoluminescence dating method. Geoarchaeol Int 12(5):479–496

Liritzis I, Zacharias N, Polymeris GS, Kitis G, Ernston K, Sudhaus D, Neumair A, Mayer W, Rappengluck MA, Rappengluck B (2010) The Chiemgau meteorite impact and tsunami event (Southeast Germany): first OSL dating. Mediterr Archaeol Archaeomet 10(4): 17–33

Liritzis I, Mavrikis D, Zacharias N, Sakalis A, Tsirliganis N, Polymeris GS (2011) Potassium determinations using SEM, FAAS and XRF: some experimental notes. Mediterr Archaeol Archaeomet 11(2): 169–178

Liritzis I, Singhvi AK, Feathers JK, Wagner GA, Kadereit A, Zacharias N, Li SH (2013a) Luminescence dating in archaeology, anthropology and geoarchaeology: an overview. Springer Briefs in Earth System Sciences

Liritzis I, Stamoulis K, Papachristodoulou C, Ioannides K (2013b) A reevaluation of radiation dose rate conversion factors. Mediterr Archaeol Archaeomet 13(3):1–15

Liritzis I, Aravantinos V, Polymeris GS, Zacharias N, Fappas I, Agiamarniotis G, Sfampa IK, Vafiadou A, Kitis G (2015) Witnessing prehistoric Delphi by luminescence dating. C R Palevol 14:219–232

Lowrie W (1990) Identification of ferromagnetic minerals in a rock by coercivity and unblocking temperature properties. Geophys Res Lett 17:159–162

Lowrie W, Fuller M (1971) On the alternating field demagnetization characteristics of multidomain thermoremanent magnetization in magnetite. J Geophys Res 76:266339–266349

Maniatis Y (2014) Radiocarbon dating of the major cultural changes in prehistoric Macedonia: recent developments. In: Stefani L, Merousis N, Dimoula A (Eds): A century of research in prehistoric Macedonia international conference proceedings 2012 205–223

Mayya YS, Morthekai P, Muraru MK, Singhvi AK (2006) Towards quantifying beta microdosimetric effects in single-grain quartz dose distribution. Radiat Meas 41:1032–1039

Murray AS, Wintle AG (2000) Luminescence dating of quartz using an improved single-aliquot regenerative-dose protocol. Radiat Meas 32:57–73

Nathan RP, Thomas PJ, Jain M, Murray AS, Rhodes EJ (2003) Environmental dose rate heterogeneity of beta radiation and its implications for luminescence dating: Monte Carlo modeling and experimental validation. Radiat Meas 37:305–313

Pavón-Carrasco FJ, Osete ML, Torta J (2010) Regional modeling of the geomagnetic field in Europe from 6000 BC to 1000 BC. Geochem Geophys Geosyst 11(Q11008):1–20

Pavón-Carrasco FJ, Rodriguez-Gonzalez J, Osete ML, Torta J (2011) A Matlab tool for archaeomagnetic dating. J Arch Sci 38(2):408–419 Pavón-Carrasco FJ, Osete ML, Torta JM, De Santis A (2014) A geomagnetic field model for the Holocene based on archaeomagnetic and lava flow data. Earth Planet Sci Lett 388:98–109

Polymeris GS, Erginal AE, Kiyak NG (2012) A comparative morphological, compositional and TL study of Tenedos (Bozcaada) and Sile aeolianites, Turkey. Mediterr Archaeol Archaeom 12(2):117–131

Prescott JR, Hutton JT (1994) Cosmic ray contributions to dose rates for luminescence and ESR dating: large depths and long-term time variations. Radiat Meas 23:497–500

Raptis KT (2011a) Archaeological evidence of ceramic production workshops in Greece (4th-15th century). DChAE 32:173–196 (in Greek with English summary)

Raptis KT (2011b) L' eredita romana nelle fornaci per la produzione di ceramica in Grecia tra il IV e il XV secolo. Rivista di Archeologia XXXV:185–191

Raptis KT (2012a) Early Christian and Byzantine ceramic production workshops in Greece: typology and distribution. Atti del IX Congresso Internazionale sulla Ceramica Medievale nel Mediterraneo 38–43

Raptis KT (2012b) Early Byzantine Plinthokerameio (brick and tile producing workshop) at the margins of the western cemetery of Thessaloniki (rescue excavation at Mazaraki, Yannitson and Kavalas strs) (in Greek with English summary) AEMTh 26 forthcoming

Raptis KT (2015a) Brick and tile producing workshops in the outskirts of Thessaloniki from 5th till 15th century: a diachronic study of the firing technology that has been continuously applied in the ceramic workshops of a large byzantine urban center.

Proceedings of 10th international congress on Medieval pottery in the Mediterranean, 493–508

Raptis KT (2015b) Seeking the marketplaces of Byzantine Thessalonike. Niš and Byzantium XIII:237–250

Roberts HM, Wintle AG (2001) Equivalent dose determinations for polymineralic fine grains using the SAR protocol: application to a Holocene sequence of the Chinese Loess Plateau. Quat Sci Rev 20: 859–863

Tema E, Fantino F, Ferrara E, Lo Giudice A, Morales J, Goguitchaichvili A, Camps P, Barello F, Gulmini M (2013) Combined archaeomagnetic and thermoluminescence study of a brick kiln excavated at Fontanetto Po (Vercelli, Northern Italy). J Archeol Sci 40(4):2025–2035

Tema E, Polymeris G, Morales J, Goguitchaichvili A, Tsaknaki V (2015) Dating of ancient kilns: a combined archaeomagnetic and thermoluminescence analysis applied to a brick workshop at Kato Achaia, Greece. J Cultural Herit 16:496–507

Tema E, Ferrara E, Camps P, Barbaro CC, Spatafora S, Carvallo C, Poidras T (2016) The Earth's magnetic field in Italy during the Neolithic period: new data from the Early Neolithic site of Portonovo (Marche, Italy). Earth Plan Sci Let 448:49–61

Vieillevigne E, Guibert P, Bechtel F (2007) Luminescence chronology of the medieval citadel of Termez, Uzbekistan: TL dating of bricks masonries. J Archeol Sci 34:1402–1416

Wagner GA (1998) Age determination of young rocks and artifacts: physical and chemical clocks in quaternary geology and archaeology. Springer, Berlin Heidelberg

Walker M (2005) Quaternary dating methods. Wiley, West Sussex Wallinga J (2002) Optically stimulated luminescence dating of fluvial deposits: a review. Boreas 31:303–322

Zhang JF, Zhou LP (2007) Optimization of the 'double SAR' procedure for polymineral fine grains. Radiat Meas 42:1475–1482

Zimmerman DW (1971) Luminescence dating using fine grains from pottery. Archaeometry 13(1):29–56

Figure captions :

Fig. 1 Early Byzantine brickyard at Yannitson Street. a Aerial view of the site. b Photos of the four kilns unearthed in the site.

Fig. 2 Rock magnetic experiments performed on representative samples from the three kilns. a Normalized IRM curves. b Stepwise thermal demagnetization of three-axis IRM. c Variation of magnetic susceptibility with temperature (k–T curves). d Lowrie–Fuller test

Fig.3 Representative Zijderveld diagrams during thermal(a) and AF(b) demagnetization. In all cases, a single component of magnetization is revealed.

Fig.4 Stereographic projection of the mean direction of the characteristic remanent magnetization (ChRM) for the three studied kilns separately. Black dots indicate the ChRM direction of the specimens while the purple dot represents the calculated mean direction for the kiln.

Fig.5 Archaeointensity determination by means of multispecimen technique. Closed (open) dots represent used (rejected) data. a MSP-DSC plot using the standard quality criterion of samples with NRM fraction greater than 0.2. b MSPDSC plot using only samples with NRM fraction between 0.65 and 0.8. The pink-shaded area represents the 95% confidence interval of the best fit slope (see text for details).

Fig. 6 Archaeomagnetic dating for the site YA using the Matlab tool for archaeomagnetic dating by Pavón-Carrasco et al. (2011). *Top* SVCs for declination, inclination and intensity calculated from the SCHA.DIF.3K model with the obtained direction and intensity of the site. *Middle* probability density functions for each element of the geomagnetic field (D, I, F). *Bottom* final age estimation calculated from the combined probability density of the three elements.

Fig.7 a Glow curves of the additive dose procedure, namely thenatural TL (NTL) along with three additive glow curves (5, 10 and 15 Gy, respectively) for the sample YA4-2. Reheats have been subtracted. b Dose-response-slope curve S of TL for the sample YA4-2, versus temperature, for the three additive doses applied. Inset additive dose growth curve for the temperature of 320 °C, for both first and second glow measurements. The arrow indicates the De value. Supra-linearity correction (I) is estimated to be zero. c De versus temperature, indicating a long plateau; for details, refer to Table 1

Fig. 8 Typical SEM backscattered image divided into four segments. For each segment, an independent 40K estimation was provided.

Fig. 9 Comparison of the new data with the predictions of the global ARCH3K.1 (light blue line) and the regional SCHA.DIF.3K (black line) geomagnetic field models as well as with other published data for the same period

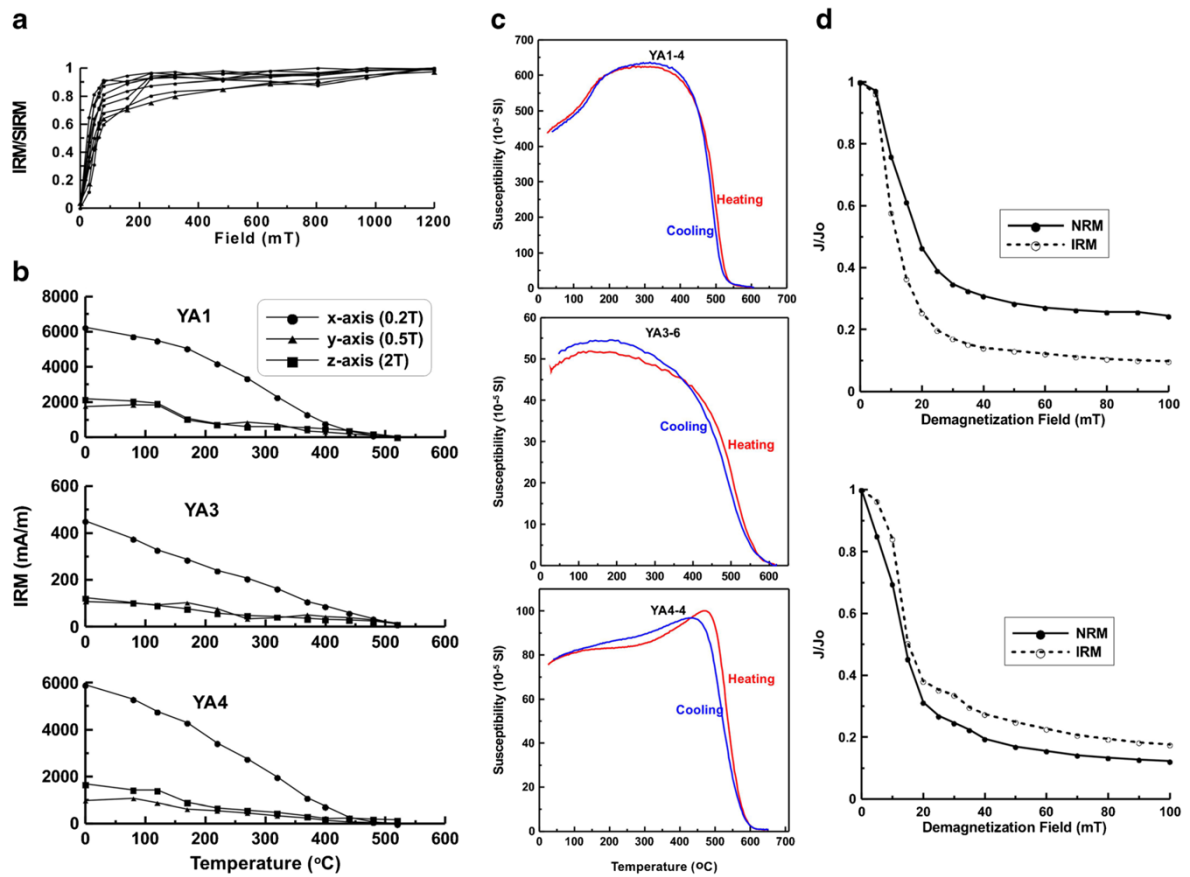Fig.10 Comparison of dating techniques for each kiln separately.
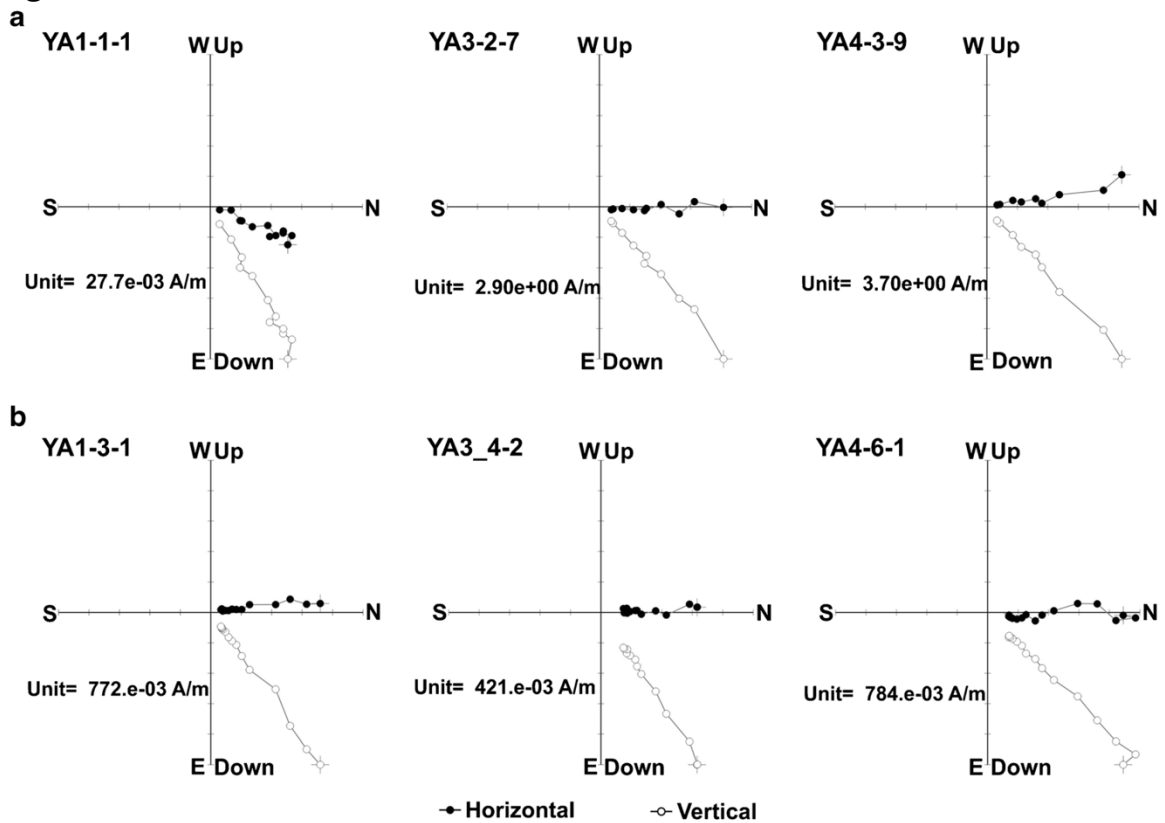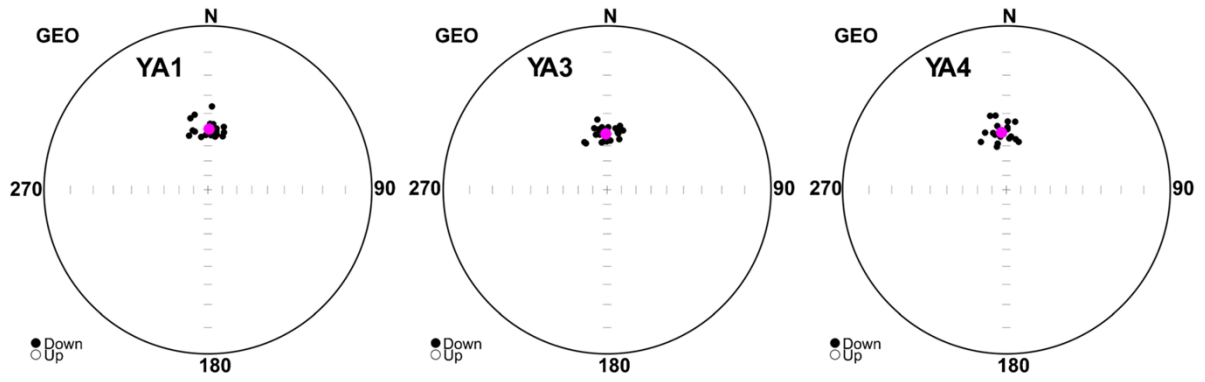
Figure 1.

Figure 2.

Figure 3.

Figure 4.
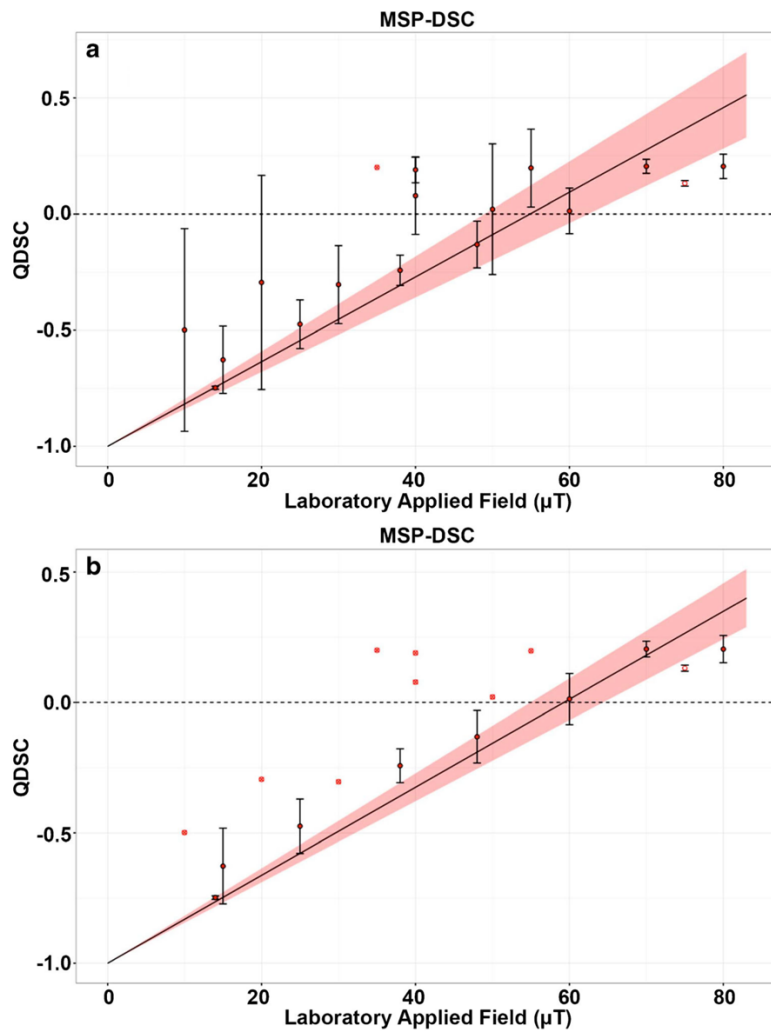
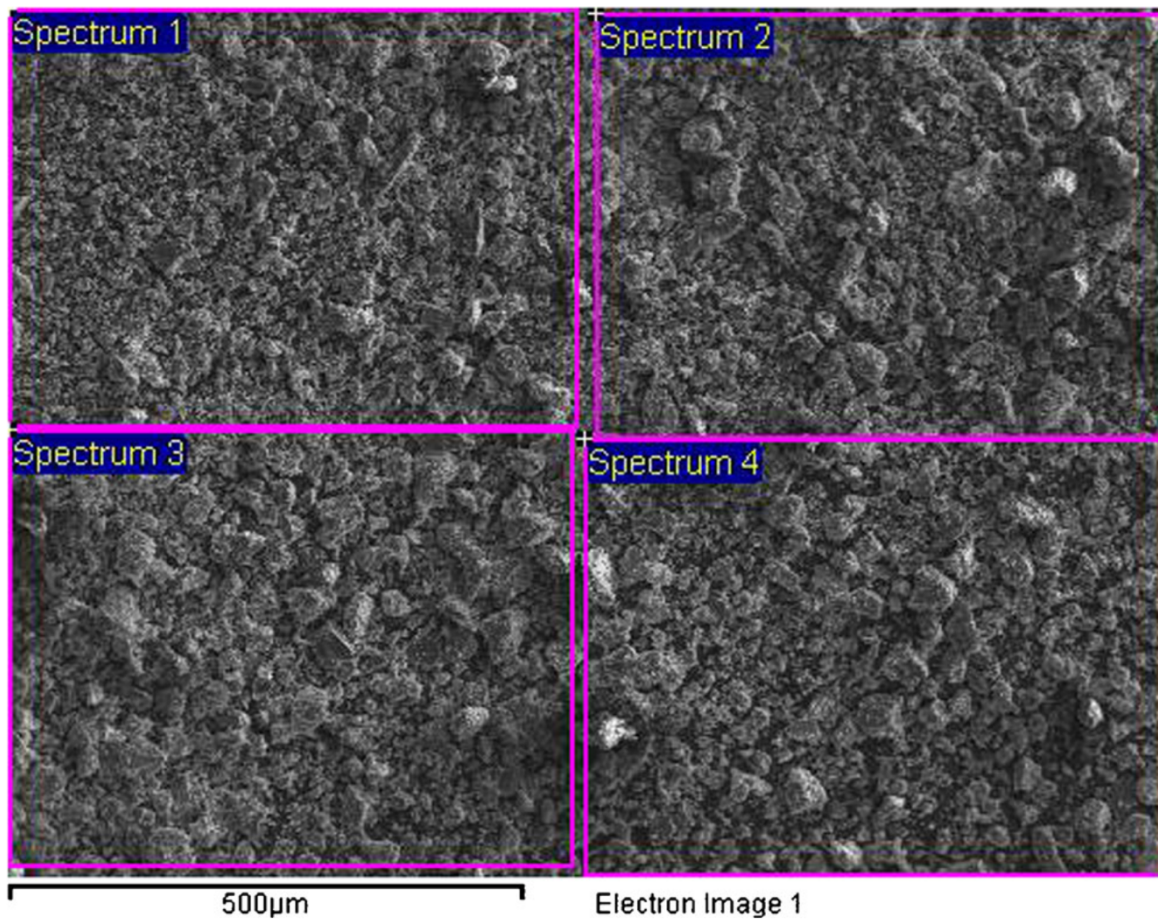**Figure 5.**
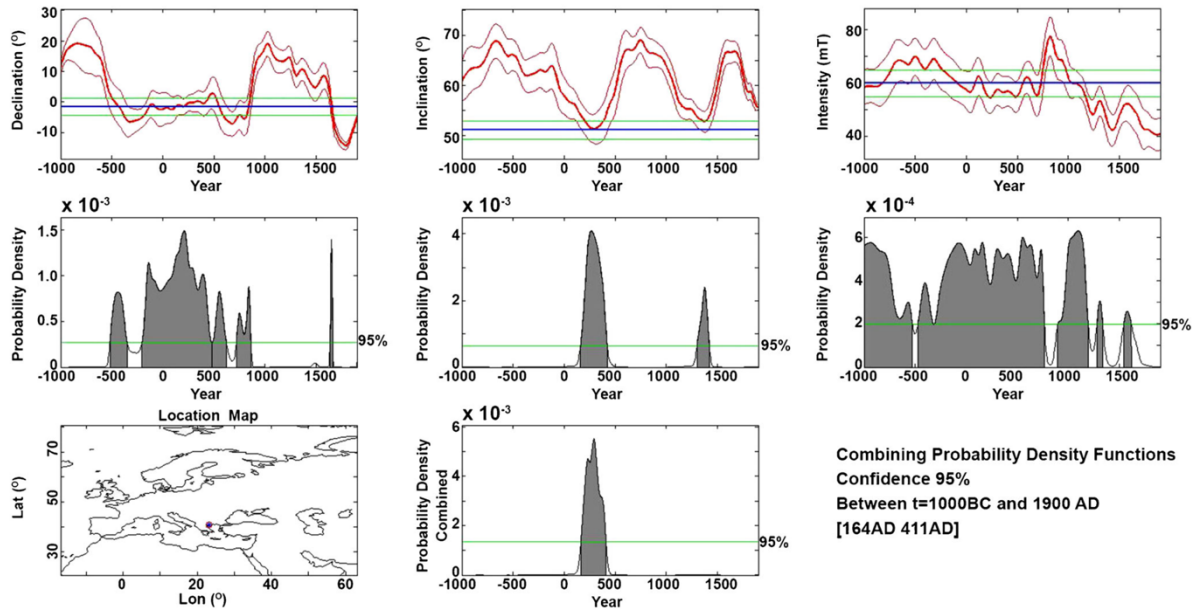
Figure 6.
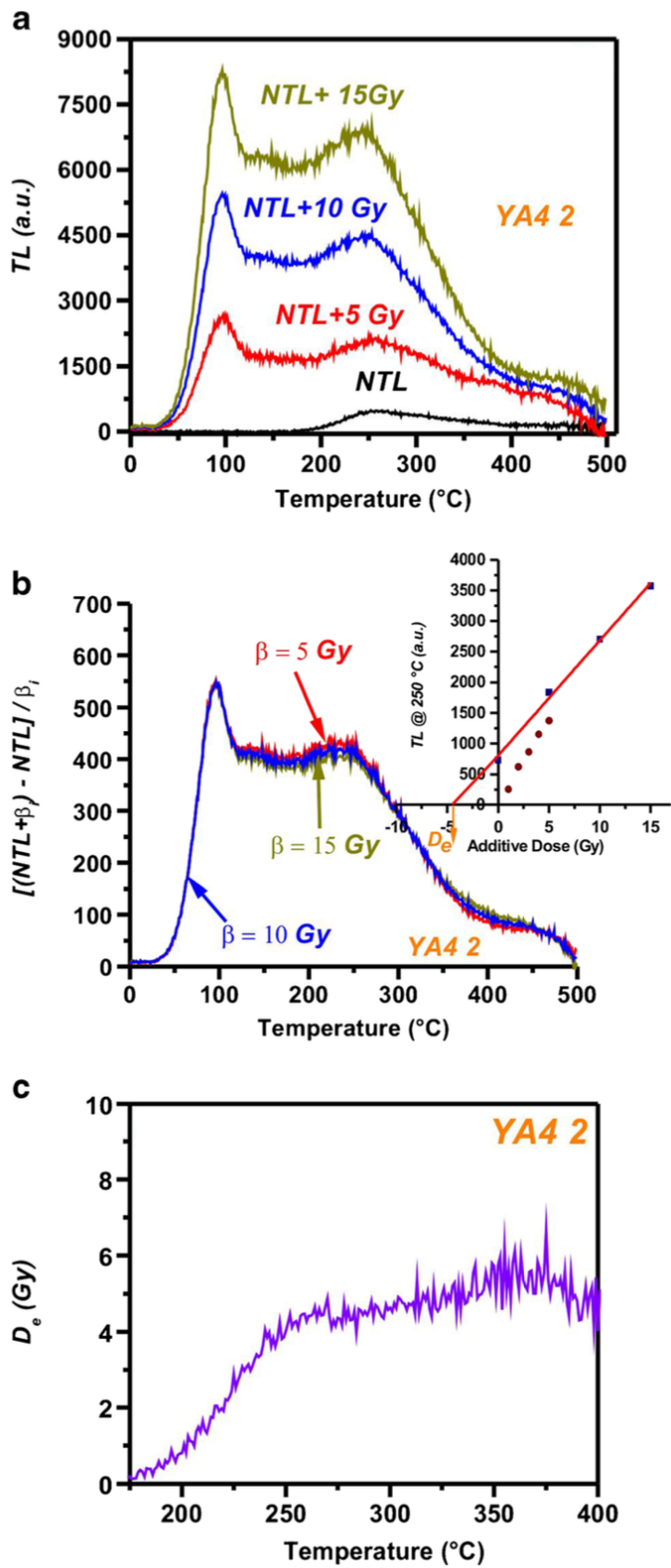
Figure 7

Figure 8.
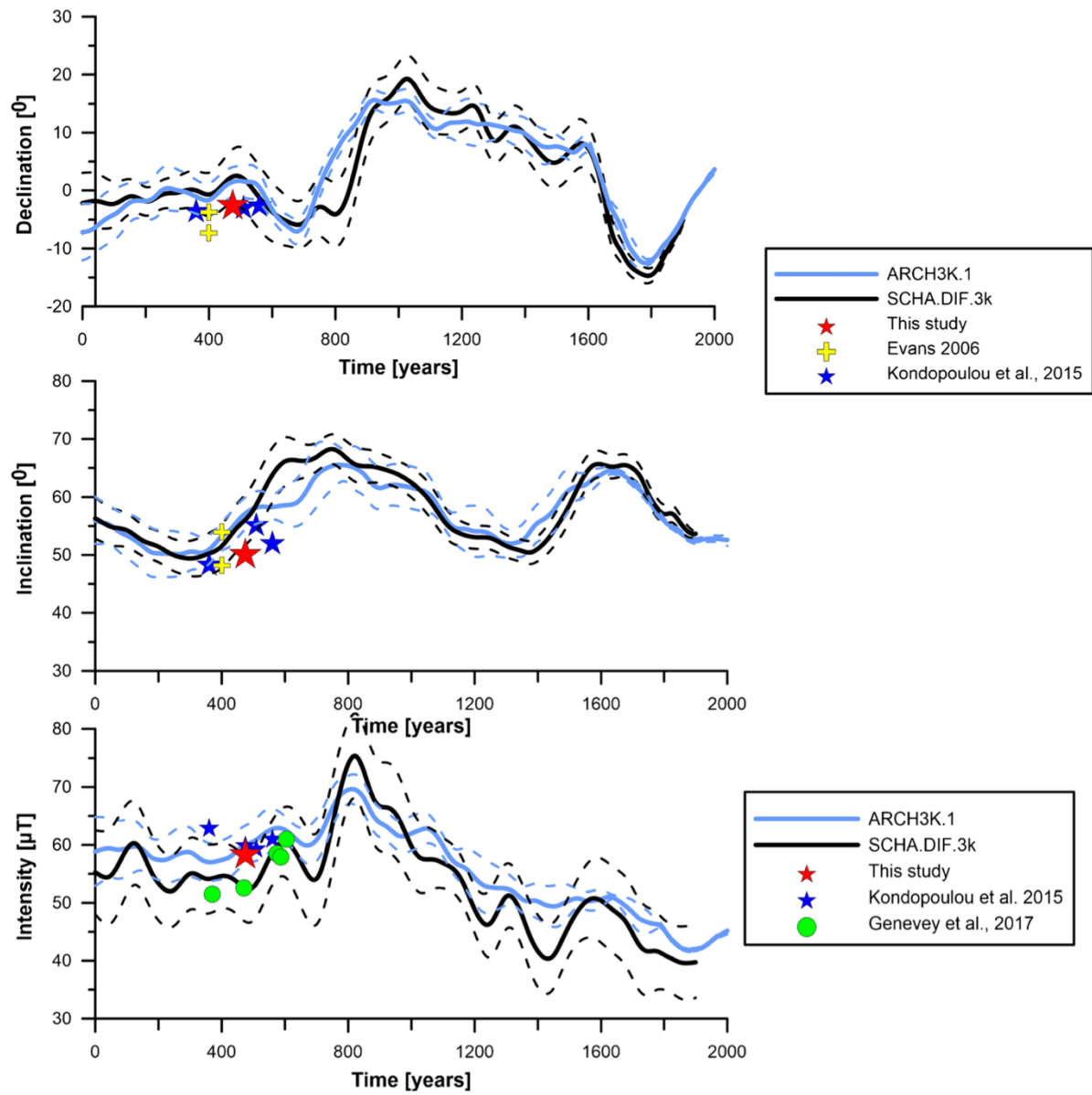
Figure 9.
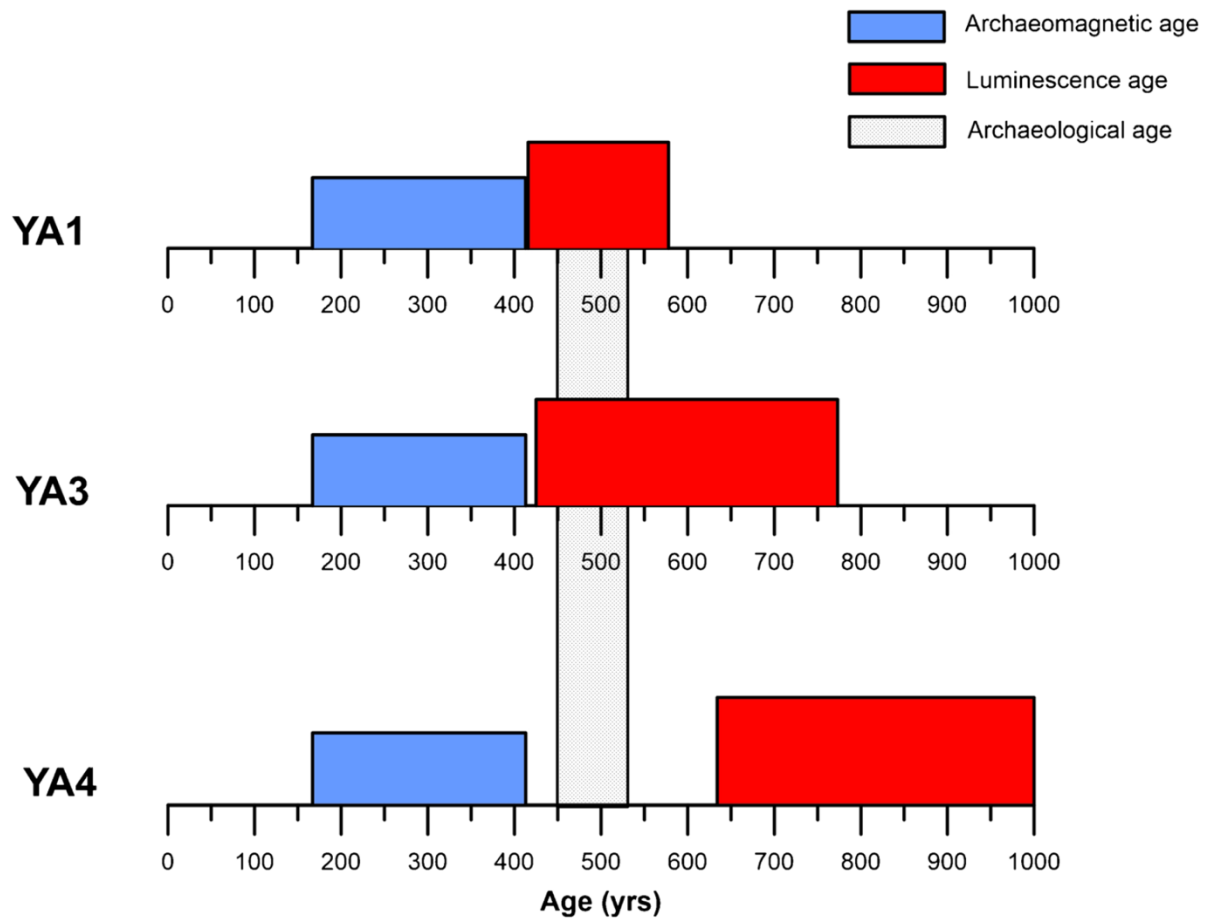
Figure 10.

Table 1 Summary of the new archaeomagnetic results. N =number of specimens; D= declination; I = inclination; α_{95} = 95% semi-angle of confidence; k = Fisher's precision parameter; N/F = number of specimens used to the total number of studied specimens during the archaeointensity experiment; F = intensity

Site	*Lat/Long*	*N*	*D (^{0})*	*I(^{0})*	*a_{95}*	*k*	*N/F*	*F(μT)*
YA1	40.7°/23.1°	21	1.1°	49.3°	3.3°	96		
YA3	40.7°/23.1°	25	358.7°	52.3°	2.9°	103		
YA4	40.7°/23.1°	21	355.2°	51.3°	3.2°	98		
MEAN	**40.7°/23.1°**	**67**	**358.4**	**51.1**	**1.8**	**96.7**	**8/17**	**59.3 ±2.1**

Table 2. A summary of the luminescence data required for age assessment of the kilns. Values in parenthesis indicate the errors on the corresponding estimation. * TL equivalent doses were corrected for anomalous fading; g values yielded were 1.37% per decade for the case of kiln YA3 and 1.83% per decade for the kiln YA4. # Dose rate estimated by using a fraction of 15% of moisture for the kiln matrix. & Dose rate and ages yielded after incorporating a correction of the K content.

Code Name	U (ppm)	Th (ppm)	K (%)	TL D_e (Gy)	TL D_e* (Gy)	ΔT (°C)	OSL D_e (Gy)	n	DR# (Gy/ka)	TL Age (BP)	OSL Age (BP)	DR& (Gy/ka)	Age& (years BP)	AGE (AD)
YA 15	8.4 (0.3)	4.8 (0.8)	2.07 (0.32)	6.60 (0.36)	6.60 (0.36)	290 – 375	-	-	4.162 (0.285)	1586 (45)	-	-	-	427
YA 17	11.2 (0.3)	3.6 (0.5)	2.41 (0.29)	6.81 (0.44)	6.81 (0.44)	300 – 360	-	-	4.397 (0.255)	1548 (58)	-	-	-	465
YA 18	3.6 (0.2)	6.2 (0.9)	2.24 (0.31)	6.35 (0.49)	6.35 (0.49)	305 – 370	-	-	4.318 (0.281)	1479 (44)	-	-	-	534
Mean dating for YA1														**475(±54)**
YA 34	3.0 (0.3)	7.5 (1.1)	5.23 (0.98)	4.88 (0.20)	5.16 (0.28)	290 – 360	5.23 (0.28)	11	6.454 (0.515)	799 (162)	811 (151)	3.889 (0.415)	1326 (189)	690
YA 35	3.1 (0.3)	6.9 (1.5)	4.93 (0.95)	4.94 (0.15)	5.22 (0.25)	280 – 340	5.32 (0.29)	11	6.188 (0.523)	844 (149)	860 (141)	3.813 (0.423)	1369 (191)	647
YA 36	3.5 (0.3)	6.0 (1.3)	5.57 (1.12)	5.77 (0.21)	6.11 (0.31)	320 – 370	-	-	6.768 (0.568)	901 (152)	-	4.131 (0.468)	1476 (180)	540
YA 38	3.9 (0.4)	11.0 (1.4)	5.45 (0.93)	5.81 (0.21)	6.13 (0.30)	280 – 360	-	-	7.386 (0.563)	830 (144)	-	4.730 (0.463)	1296 (172)	720
YA 310	4.0 (0.4)	8.9 (1.2)	5.14 (1.02)	4.91 (0.16)	5.19 (0.25)	290 – 355	5.31 (0.24)	12	6.213 (0.587)	833 (129)	872 (155)	4.553 (0.487)	1348 (176)	668
Mean dating for YA3														**599(±174)**
YA 42	2.0 (0.3)	11.9 (1.9)	5.09 (1.03)	4.54 (0.19)	4.97 (0.29)	250 – 310	5.26 (0.21)	11	6.456 (0.399)	753 (174)	812 (159)	8.039 (0.499)	1179 (214)	837
YA 43	3.6 (0.3)	8.6 (1.4)	5.25 (0.99)	4.96 (0.27)	5.45 (0.39)	320 – 365	5.62 (0.23)	11	6.836 (0.402)	782 (181)	822 (145)	8.515 (0.502)	1198 (202)	818
YA 46	2.5 (0.3)	7.2 (1.5)	4.31 (1.03)	4.13 (0.46)	4.47 (0.66)	250 - 325	-	-	5.471 (0.345)	807 (196)	-	6.813 (0.445)	1267 (223)	749
YA 47	2.2 (0.4)	10.9 (1.8)	5.17 (0.88)	4.35 (0.15)	4.75 (0.23)	260 – 325	-	-	6.466 (0.412)	725 (155)	-	8.053 (0.512)	1139 (199)	877
YA 48	2.7 (0.3)	9.1 (1.5)	3.66 (1.18)	3.72 (0.16)	4.09 (0.23)	250 - 280	4.62 (0.19)	11	5.211 (0.386)	769 (198)	887 (142)	6.491 (0.436)	1147 (207)	869
Mean dating for YA4														**826(±192)**

Table 3. Mean values and the corresponding standard deviations expressed in terms of error percentage for all major elements.

Code	Na	Error Na (%)	Mg	Error Mg (%)	Si	Error Si (%)	K	Error K (%)	Fe	Error Fe (%)
YA3-4	1.08	19.44	1.74	16.09	61.01	2.07	5.82	20.79	12.25	14.45
YA3-5	1.3	24.62	1.78	12.36	63.77	2.62	4.93	10.75	11.69	12.32
YA3-6	1.99	22.11	2.54	9.06	52.53	2.23	5.57	12.75	13.40	10.82
YA3-8	1.34	5.22	2.41	10.79	53.55	1.77	5.45	6.06	13.15	10.27
YA3-10	1.77	31.64	2.45	16.33	53.85	2.49	5.15	19.61	13.12	10.52
YA4-2	0.94	38.30	2.09	21.05	56.45	3.10	5.38	10.78	12.54	11.08
YA4-3	1.71	23.98	2.08	20.19	50.90	3.20	5.48	12.59	13.42	4.92
YA4-6	1.77	14.69	2.20	28.64	54.10	5.16	3.32	22.29	11.72	7.51
YA4-7	1.51	35.10	2.07	28.50	56.03	3.68	5.17	17.02	11.64	13.40
YA4-8	1.17	33.33	2.03	23.15	52.61	4.41	3.66	24.04	13.96	6.73